Original Research Article
Non-tipping Tube in Quiescent Water Based on Static Moment Equilibrium

ABSTRACT

In mechanics and engineering applications, the study of rigid body stability holds significant importance. The method of static moment equilibrium is a critical tool for analyzing the stability of rigid bodies. In this paper, a simple and practical non-tipping tube device is constructed, which can maintain balance in quiescent water even under horizontal external force. The functional relationship between the inclination angle of the tube and the external force was obtained through theoretical analysis, and the experimental data modified the theoretical model. The device can detect external force up to 4.11±0.04 N (P=0.95). This intuitive experimental device has potential applications in physics teaching and the fields of wind detection engineering.

Keywords: Moment equilibrium; Gravitational torque; Three-axis sensor; Static stability

1. INTRODUCTION

Stability is a common phenomenon in nature, for example, a small ball would maintain stability at the center of a bowl in the absence of external forces, and a tumbler toy would remain upright when placed on a horizontal table [1-2]. The investigation of the factors contributing to the stability of these objects has significantly advanced the progress and utilization of mechanics (e.g., [3-5]). Simultaneously, the recent surge in machine learning has significantly enriched the research work in the field of mechanics[6, 7]. The equilibrium characteristics of a mechanical system can be analyzed based on the principle of minimum potential energy [8-9].

The non-tipping tube is a classical system equilibrium problem that has attracted the attention of numerous researchers [10-11], and references therein. The equilibrium characteristics of the device can be briefly analyzed by using the knowledge of static moment equilibrium of rigid body mechanics (e.g., [12-13]). This type of research may possess practical application value in areas such as bioengineering [14], textile engineering [15], ocean engineering design [16-17], and so on. Simultaneously, by investigating this issue, we can further enhance our comprehension of the mechanical equilibrium problem, which holds a certain reference value in physics teaching.

In this paper, a non-tipping tube device is designed, which can be capable of maintaining balance and stability in quiescent water under horizontal external force. The device enables real-time monitoring of the inclination angle through a wireless three-axis sensor in the tube. The buoyancy center can be adjusted via tube immersion ratio in water. The gravitational torque, buoyant torque, water plane restoring torque, and external force torque can be discussed through the analysis of the rigid body model. Finally, a quantitative functional relationship between external force and the inclination angle is established, which is further modified and verified through experiments.

2. METHODOLOGY AND EXPERIMENTAL DETAILS

2.1 Experimental Apparatus

Experimental instruments: Bombo STEAM programming robot ET841, water, large sink, plastic tube, 3-axis wireless inclinometer sensor, NaCl crystals, vernier caliper, glue gun, glue, high strength thin wire, rubber band, sealing ring, sealing cover, raw material belt, high precision electronic balance, spring dynamometer.

2.2 Static Moment Equilibrium Fundamentals

Figure 1 shows the schematic diagram of the non-tipping tube device. The tube can be treated as a rigid tube with its bottom end fixed at the hinge point by the high-strength thin wire and glue. Therefore, it can rotate around the hinge point O in the vertical plane. As shown in Fig. 1, The center of gravity of the hollow tube will be toward the bottom once a specific quantity of NaCl crystals has been introduced. Notice that the direction of gravity always acts vertically downward, while the direction of buoyancy always acts vertically upward. When the tube is subjected to horizontal external, as shown in Fig.1, it will induce a specific inclination angle, leading to the generation of gravitational torque ($\overrightarrow{M_G} = \overrightarrow{r_G} \times \overrightarrow{G}$), buoyant torque ($\overrightarrow{M_b} = \overrightarrow{r_b} \times \overrightarrow{F_b}$), external torque ($\overrightarrow{M_e} = \overrightarrow{r_e} \times \overrightarrow{F_e}$), and water plane restoring torque ($\overrightarrow{M_{wp}}$). The four torques can achieve static moment equilibrium at the hinge point O , thereby ensuring the stability of the tube. As the external force increases, the angle of the tube will further increase, leading to a higher immersion ratio of the tube in the water. Hence, the buoyancy is enhanced, leading to a significant increase in the buoyant torque. Meanwhile, the external force on the tube is mitigated by reducing the exposed area, resulting in increased stability of the tube.

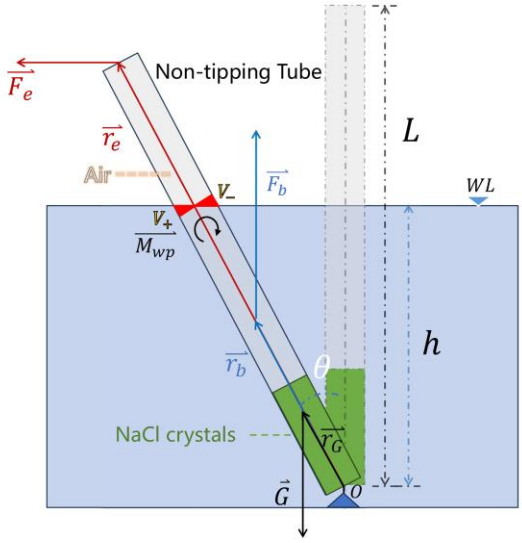

Fig.1. Schematic diagram of the non-tipping tube device.

2.3 Theoretical Analysis of Static Moment Equilibrium

As shown in Figure 1, the length of the tube is denoted as L , and the submerged length of the tube in a vertical position is denoted as h . When the tube is at an angle of θ , the buoyancy of the tube in water is $F_b = \rho g V = \rho g A h \sec\theta$, where A represents the tube cross-section area and ρ represents the density of the water. Mathematically, the water plane restoring torque ($\overrightarrow{M_{wp}}$) is generated by the couple moment generated by both the positive buoyancy force of the submerged wedge (V_+) and the negative buoyancy force of the emerged wedge (V_-) [18-19], as illustrated in Fig. 1, and can be formulated as

$$M_{wp} = \rho g I_A \sin\theta (1 + \frac{1}{2}\tan^2\theta)$$

where $I_A = \frac{\pi D^4}{64}$ is the second moment of the tube's cross-section area, in which D is the diameter of the tube. Analyzing the resultant torque on the tube, we define that its positive direction is perpendicular to the plane of the paper and points to it. Thus,

$$\begin{aligned}\overrightarrow{M} &= \overrightarrow{M_G} + \overrightarrow{M_b} + \overrightarrow{M_{wp}} + \overrightarrow{M_e} \\ &= \overrightarrow{r_G} \times \overrightarrow{G} + \overrightarrow{r_b} \times \overrightarrow{F_b} + \overrightarrow{M_{wp}} + \overrightarrow{r_e} \times \overrightarrow{F_e} \\ &= -\left|\overrightarrow{r_G}\right|\left|\overrightarrow{G}\right|\sin(\pi - \theta) + \left|\overrightarrow{r_b}\right|\left|\overrightarrow{F_b}\right|\sin\theta + \rho g I_A \sin\theta(1 + \frac{1}{2}\tan^2\theta) - \left|\overrightarrow{r_e}\right|\left|\overrightarrow{F_e}\right|\sin(\frac{\pi}{2} - \theta)\end{aligned}$$

When the tube is stabilized, the net torque acting on it becomes zero. The above formula can be simplified as follows.

$$0 = -\left|\vec{r_G}\right|\left|\vec{G}\right|\sin\theta + \left|\vec{r_b}\right|\left|\vec{F_b}\right|\sin\theta + \rho g I_A \sin\theta(1+\frac{1}{2}\tan^2\theta) - \left|\vec{r_e}\right|\left|\vec{F_e}\right|\cos\theta$$

$$= -r_G G\sin\theta + \frac{h}{2\cos\theta}\rho g A\frac{h}{\cos\theta}\sin\theta + \rho g\frac{\pi D^4}{64}\sin\theta(1+\frac{1}{2}\tan^2\theta) - LF_e\cos\theta$$

Hence, the external force F_e can be expressed as follows.

$$F_e = \frac{\rho g A h^2 \tan\theta\sec^2\theta}{2L} + \frac{\rho g\pi D^4\tan\theta}{64L}(1+\frac{1}{2}\tan^2\theta) - \frac{r_G G\tan\theta}{L}$$

Let $a = \frac{\rho g A h^2}{2L}$, $b = \frac{\rho g\pi D^4}{64L}$, $c = \frac{r_G G}{L}$, we obtain,

$$F_e = a\tan\theta\sec^2\theta + b\tan\theta(1+\frac{1}{2}\tan^2\theta) - c\tan\theta \qquad (1)$$

Equation (1) represents the theoretical functional correlation between the horizontal external force F_e and the inclination angle θ of the non-tipping tube device. The other measured parameters, $D = 43.00\ mm$, $L = 250.0\ mm$, $h = 125.0\ mm$, $r_G = 63.0\ mm$, $A = 1452.2\ mm^2$ and $G = 0.8878\ \mathrm{N}$, are substituted into the expressions for $a = \frac{\rho g A h^2}{2L}$, $b = \frac{\rho g\pi D^4}{64L}$, $c = \frac{r_G G}{L}$ while taking $g = 9.807\ \mathrm{m/s^2}$ and $\rho = 0.9972\times10^3\ \mathrm{kg/m^3}$. It can be derived that $a = 0.4438\ \mathrm{N}$, $b = 0.0066\ \mathrm{N}$ and $c = 0.2237\ \mathrm{N}$. Therefore, by substituting the values of a, b and c into equation (1),

$$F_e = 0.4438\tan\theta\sec^2\theta + 0.0066\tan\theta(1+\frac{1}{2}\tan^2\theta) - 0.2237\tan\theta \qquad (2)$$

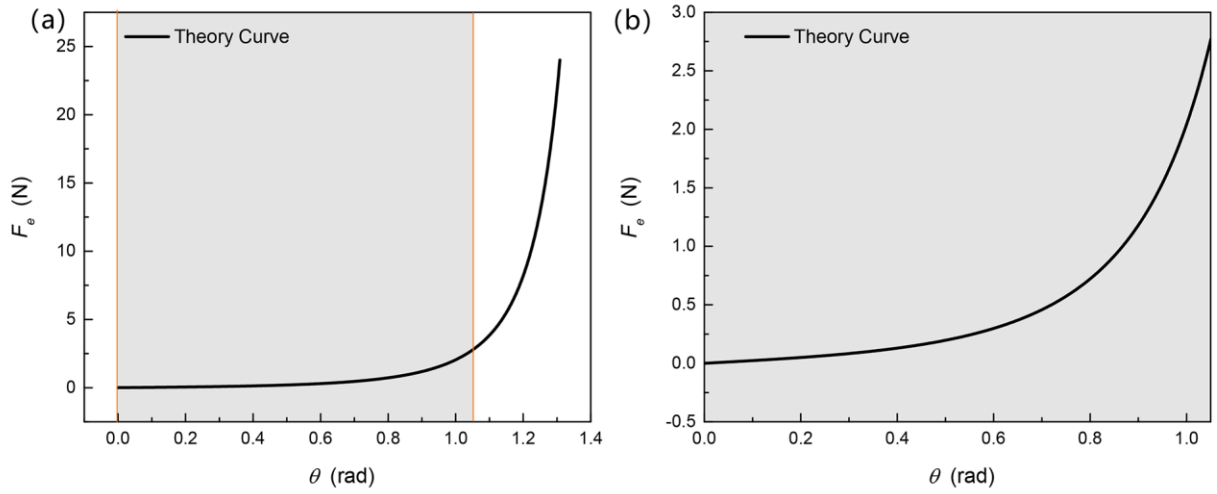

Fig. 2. (a) Theoretical curve of the horizontal external force *versus* the inclination angle. (b) The enlargement figure of the gray area in (a).

The theoretical function image of F_e *versus* θ is shown in Fig. 2 (a). As depicted in the figure, the static moment equilibrium of the device exhibits half of a typical Pitchfork bifurcation diagram [20]. When considering the F_e in the opposite direction, it would form a complete Pitchfork bifurcation diagram. The gray area is the theoretical measurable area, and the maximum inclination angle θ is up to 60 degrees (1.05 rad). Since the tube would be completely submerged in water without being affected by the external while θ is more than 1.05 rad, which makes the tube device equipped with self-protection capabilities in super windy conditions. Figure 2(b) is an enlarged view of the gray area in Fig. 2(a). It can be seen from Fig. 2(b) when the tube is initially in a vertical state, even a weak F_e can cause a noticeable θ. When the inclination angle θ exceeds 0.8 radians, the θ increases slowly with the rising.

A new physical quantity S (N/rad) is then defined to characterize the stability of the non-tipping tube at any given inclination angle θ. The value of S can be derived by taking the first derivative of the function F_e with respect to the variable θ, expressing as $S = \frac{dF_e}{d\theta}$. Hence,

$$S = a(1+2\sin^2\theta)\sec^4\theta + b(\frac{3}{2}\tan^2\theta+1)\sec^2\theta - c\sec^2\theta \quad (3)$$

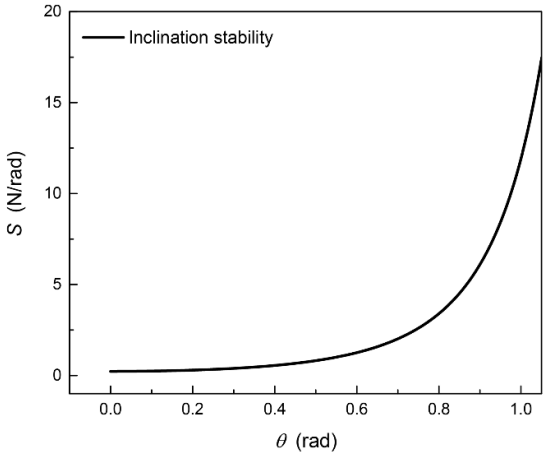

Fig. 3. Variation of theoretical stability with tube inclination angle.

The stability of the non-tipping tube S *versus* θ is shown in the above Fig. 3. It is evident that as the θ of the tube increases, so does the stability S, indicating a higher level of tube stability and increased external force resistance, i.e., the sensitivity of the θ diminishes as F_e fluctuates. On the contrary, when the tube is vertical or less than 0.6 radians, even a slight force disturbance will result in a significant increase in tube inclination, as confirmed by the subsequent experiments.

2.4 Device Preparation

1)The plastic tube, sealing ring, and sealing cover were designed by the Bombo STEAM programmed robot ET841 and made by a plastics company.
2)Using a vernier caliper to measure the length *L*=250.0±0.08 mm (P=0.68) and the diameter *D*=43.0±0.02 mm (P=0.68) of the tube. See Supplemental material part 1 for calculation and analysis of measurement uncertainty.
3)Seal the bottom of the plastic hollow tube with a sealing cover by a glue gun and fix a high-strength short thin wire in the center of the bottom. Then, wrap the raw material belt around the bottom sealing ring for secondary sealing to enhance the sealing effectiveness.
4)Place a thin layer of NaCl crystals in the tube, followed by positioning a 3-axis wireless inclinometer sensor horizontally as shown in the Fig. 4(a). The wireless sensor is connected to the computer via Bluetooth and is capable of real-time recording of current 3D angle information, as depicted in Fig. 4(b). Then, add an appropriate amount of NaCl crystals to fully cover the sensor and use a sealing ring to compact the crystals, ensuring a horizontal solid layer. Record the thickness of the solid layer for consistency in future experiments, and finally cover the top of the tube with another sealing ring with a thin wire in the center.

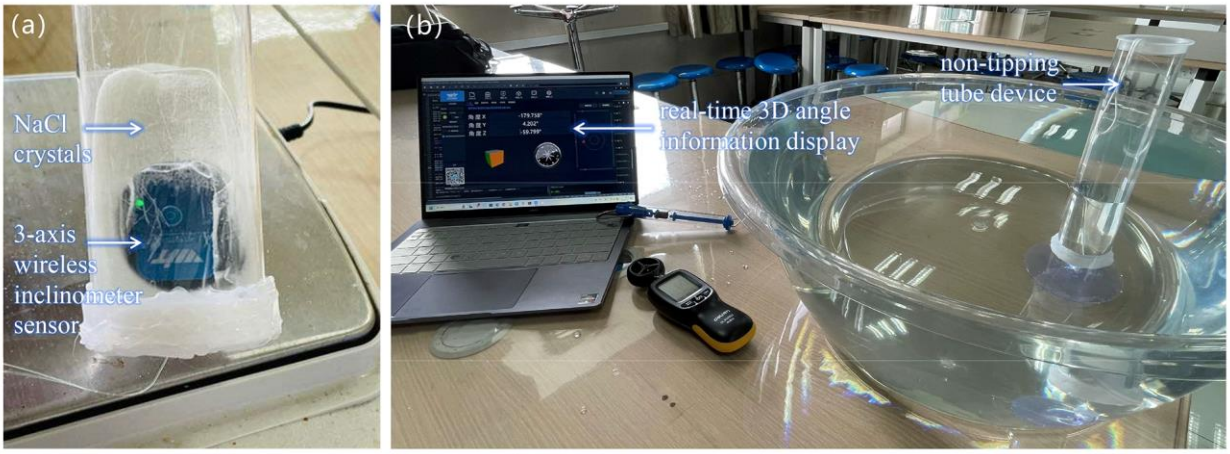

Fig. 4. (a) The interior diagram of the tube. (b)The computer displays real-time 3D angle information from the sensor.

5)Using a high-precision electronic balance to weigh the mass of the entire tube m=90.53±0.02 g (P=0.68).
6)The center of gravity position of the entire tube is determined by using the suspension method with only a rubber band, thus measuring r_G=63.00±0.08 mm (P=0.68). The NaCl-air ratio in the tube allows for handy adjustment of the center of gravity.
7)Hang the short thin wire from the bottom of the tube onto the chuck attached to the base of the large sink. Make sure that the wire is as short as possible to ensure that the hinge point O of the tube remains unchanged.
8)Start adding water to the large sink until the tube can stand vertically, then add a 1-2 cm layer of water to enhance stability. Hence, the buoyancy center can be conveniently adjusted by the sinking degree of the tube in the water. Gently push the tube, it should quickly return to its vertical position.

2.5 Experimental Procedures

1)The length of the tube immersed in water is measured to be h=125.0±0.1 mm (P=0.68), and the distance between the center of buoyancy and the hinge point O can be calculated as $r_b = \frac{h}{2\cos\theta}$, as depicted in Fig. 1.

2)After stabilizing the tube vertically, a spring dynamometer with an accuracy of 0.02 N is attached to the thin wire at the top. The tube is then pulled horizontally to record the sensor's inclination data θ under different tension forces until it is almost completely submerged in water. The tension force here is designed equivalent to the horizontal external force F_e. The experiment was repeated 3 times to minimize measurement error and enhance data accuracy. The experiment data are shown in Table 1. in the RESULTS AND DISCUSSION part.

3)Analyze the data between F_e and inclination angle θ in step 2) to revise equation (1). More information of experimental conditions and precautions can be found in Supplemental material part 2.

3. RESULTS AND DISCUSSION

The data obtained by step 2) of 2.5 are as follows:

Table 1. Corresponding data of horizontal tension force and inclination angle

F_e (N)	0	0.04	0.06	0.08	0.10	0.12	0.16	0.20	0.24	0.28	0.32	0.38
θ_1 (rad)	0.00	0.39	0.42	0.46	0.48	0.50	0.54	0.58	0.61	0.63	0.66	0.69
θ_2 (rad)	0.00	0.33	0.40	0.43	0.45	0.49	0.53	0.57	0.60	0.63	0.64	0.67
θ_3 (rad)	0.00	0.32	0.38	0.43	0.45	0.49	0.54	0.57	0.60	0.63	0.65	0.68
$\overline{\theta}$ (rad)	0	0.35	0.4	0.44	0.46	0.49	0.54	0.57	0.61	0.63	0.65	0.68
F_e (N)	0.44	0.50	0.56	0.62	0.72	0.82	0.92	1.02	1.32	1.52	1.72	2.02
θ_1 (rad)	0.71	0.73	0.75	0.77	0.79	0.82	0.85	0.87	0.88	0.90	0.91	0.93
θ_2 (rad)	0.69	0.73	0.74	0.76	0.78	0.80	0.83	0.85	0.88	0.91	0.92	0.93
θ_3 (rad)	0.70	0.72	0.74	0.76	0.78	0.81	0.83	0.84	0.89	0.91	0.93	0.93
$\overline{\theta}$ (rad)	0.70	0.73	0.74	0.76	0.78	0.81	0.83	0.85	0.88	0.90	0.92	0.93

Table 1. gives the experimental data of horizontal external force F_e and the tube inclination θ. All data are deducted from background errors. The $\overline{\theta}$ in chart represents the mean value of three measurements of θ to minimize measurement error. The data of $\overline{\theta}$ were plotted in the Fig. 5 as red solid points. Based on the obtained theoretical equation (2), actual measurements and other potential factors may result in certain variations in the values of a and c. The magnitude of b is approximately two orders of magnitude smaller than that of a and c, thus the impact of changes in

b can be disregarded. Therefore, two parameters A and C can be introduced for fitting adjustments to the values a and c. Therefore, the equation

$$F_e = (0.4438 + A)\tan\theta\sec^2\theta + 0.0066\tan\theta(1+\frac{1}{2}\tan^2\theta) - (0.2237 + C)\tan\theta$$

was utilized to fit the experimental data points in Fig. 5. The Levenberg-Marquardt algorithm was employed to obtain the fitting results, as depicted by the red fitting curve in Fig. 5. The red curve represents the actual experimental function of F_e and θ.

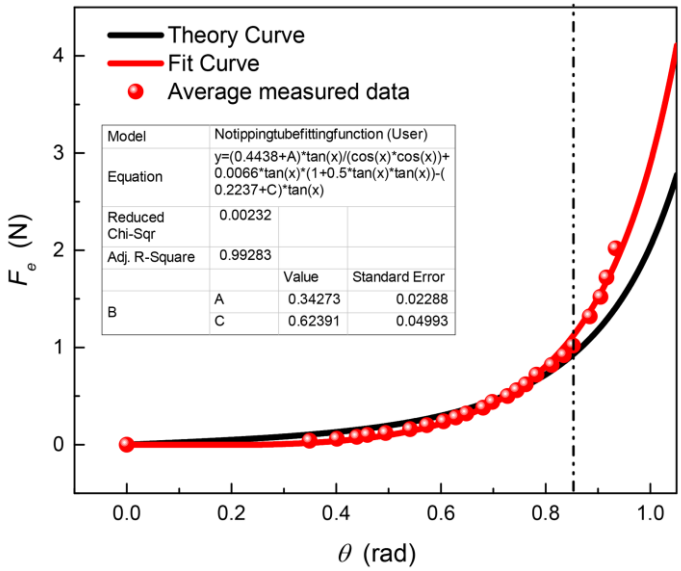

Fig. 5. The actual relationship between the horizontal external force and the tube inclination angle.

It can be seen from Fig. 5 that the data can perform very good fitting. The Adjusted R-Square is 0.99283, indicating that the function model has high accuracy. From Fig.5, the red curve indicates that the maximum F_e value can reach the upper limit of 4.11 N with uncertainty of ±0.04 N (P=0.95) according to analysis of synthetic uncertainty in the Supplemental material part 1. The values of A and C in the fitting function, as shown in the table of Fig. 5, are determined to be 0.3427 and 0.6239 respectively. Therefore, it can be concluded that the actual experimental function image satisfies the following equation (4).

$$F_e = 0.7865\tan\theta\sec^2\theta + 0.0066\tan\theta(1+\frac{1}{2}\tan^2\theta) - 0.8476\tan\theta \qquad (4)$$

To ensure the validity of the experiment and the reliability of equation (4), a double-blind verification was carried out. After applying a force of 1 N, the experiment yielded an inclination measurement of 47.80 degrees, while the calculation from equation (4) resulted in an inclination of 0.83 radians (47.73 degrees), demonstrating the high reliability of the equation.

Simultaneously, to contrast the disparity between the experimentally fitted curve and the theoretically calculated curve, both are plotted in Fig. 5 for intuitive comparison. As depicted in the figure, for θ less than 0.85 radians, the discrepancy between the two curves is negligible. However, for θ exceeding 0.85 radians, the experimental F_e surpasses the theoretical calculation value. The primary factor for this phenomenon is that when the θ exceeds 0.85 radians, the hinge point O ceases to remain stationary and undergoes a slight displacement. This slight displacement will cause the tube to experience a counteracting force opposite to the direction of the F_e, resulting in a greater F_e than the theoretical value at the same inclination. The revised values of A and C are large due to the same reason.

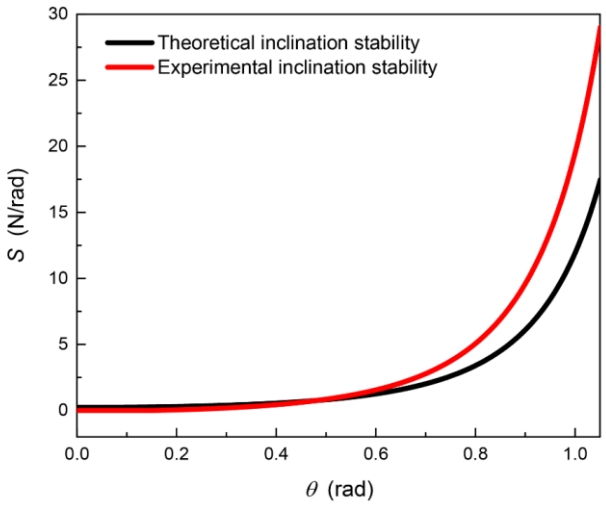

Fig. 6. Theoretical and experimental inclination stability curves.

Furthermore, when comparing the stability of the two at any given inclination angle as depicted in Fig. 6, it is evident that the actual tube exhibits a higher level of stability. The dynamic characteristics of the tube submerged in water are not elaborated upon here, as this process entails surface wave disturbances, water turbulence, and other influencing factors. Moreover, a more comprehensive simulation analysis is required involving fluid mechanics and aerodynamics [12, 20-21].

4. CONCLUSION

In this paper, a simple and practical non-tipping tube device is constructed based on the principle of static moment equilibrium. The device can maintain balance in quiescent water even under horizontal external force. The tube allows for handy adjustment of the center of gravity and the buoyancy center, with the inclination angle recorded by the three-axis sensor in the tube. The angle of the vertical tube θ will increase with the horizontal external force F_e, and as the θ increases, the tube exhibits greater stability. This result is supported by both theoretical analysis and experimental data. Meanwhile, the precise functional relationship equation (4) is derived from the theoretical analysis and modified by the experimental data, which is confirmed by the double-blind verification. The device can detect external force up to 4.11±0.04 N (P=0.95). This intuitive experimental device can be used as a demonstration experiment for teachers to expound the idea of static moment equilibrium and it has potential applications in the fields of wind detection engineering.

Disclaimer (Artificial intelligence)

Author(s) hereby declare that NO generative AI technologies such as Large Language Models (ChatGPT, COPILOT, etc.) and text-to-image generators have been used during the writing or editing of this manuscript.

REFERENCES

1. David Halliday, Robert Resnick, Jearl Walker. Fundamentals of physics. John Wiley & Sons; 2013.
2. Michael E Plesha, Gary L Gray, Francesco Costanzo. Engineering Mechanics: Statics. McGraw-Hill Higher Education New York, NY, USA; 2010.
3. A Luévanos Rojas. Method of structural analysis for statically indeterminate beams, International Journal of Innovative Computing. Information and Control. 2012;8(8):5473-5486.
4. Mohammad Jafari, Partha P Sarkar. wind-induced response characteristics of a yawed and inclined cable in ABL wind: Experimental-and numerical-model based study. Engineering Structures. 2020; 214:110681.
5. N. Han, P.P. Lu. Nonlinear dynamics of a classical rotating pendulum system with multiple excitations. Chinese Physics B 2020; 29(11): 110502.
6. Aman Garg, M-O Belarbi, Abdelouahed Tounsi, L. Li, Ankit Singh, Tanmoy Mukhopadhyay. Predicting elemental stiffness matrix of FG nanoplates using Gaussian Process Regression based surrogate model in framework of

layerwise model. Engineering Analysis with Boundary Elements. 2022; 143: 779-795.
7. D. M. Sekban, E.U. Yaylacı, M.E. Özdemir, Murat Yaylacı, Abdelouahed Tounsi. Investigating Formability Behavior of Friction Stir-Welded High-Strength Shipbuilding Steel using Experimental, Finite Element, and Artificial Neural Network Methods. Journal of Materials Engineering and Performance. 2024.
8. Henry L Langhaar. Energy methods in applied mechanics. Courier Dover Publications; 2016.
9. Davide Bigoni. Extremely Deformable Structures. Springer Vienna, Vienna; 2015.
10. Terrence Toepker, Archimedes Revisited and Beyond, The Physics Teacher. 2023;61(9): 780-784.
11. Y. Z. Liu, J. W. Zu. Stability and bifurcation of helical equilibrium of a thin elastic rod. Acta Mechanica. 2004;167(1): 29-39.
12. Varghese Mathai, Laura AWM Loeffen, Timothy TK Chan, Sander Wildeman. Dynamics of heavy and buoyant underwater pendulums. Journal of Fluid Mechanics. 2019; 862:348-363.
13. Timothy Bretl, Zoe McCarthy. Quasi-static manipulation of a Kirchhoff elastic rod based on a geometric analysis of equilibrium configurations. The International Journal of Robotics Research. 2014;33(1):48-68.
14. Prashant K. Purohit. Plectoneme formation in twisted fluctuating rods. Journal of the Mechanics and Physics of Solids. 2008;56(5):1715-1729.
15. W. B. Fraser, D. M. Stump. The equilibrium of the convergence point in two-strand yarn plying. International Journal of Solids and Structures. 1998;35(3):285-298.
16. C. L. Lu, N. C. Perkins. Complex spatial equilibria of u-joint supported cables under torque, thrust and self-weight. International Journal of Non-Linear Mechanics. 1995;30 (3): 271-285.
17. Sangrok Jin, Jihoon Kim, Jangho Bae, TaeWon Seo, Jongwon Kim, Design. modeling and optimization of an underwater manipulator with four-bar mechanism and compliant linkage. Journal of Mechanical Science and Technology. 2016;30(9):4337-4343.
18. Mohammed Khair Al-Solihat, Meyer Nahon. Nonlinear hydrostatic restoring of floating platforms. Journal of Computational and Nonlinear Dynamics. 2015;10(4):041005.
19. Adrian Biran, Rubén López-Pulido. Ship hydrostatics and stability. Butterworth-Heinemann; 2013.
20. Mohammed Khair Al-Solihat. Nonlinear static and dynamic behaviors of partially and fully submerged rod pendulums in quiescent water. Nonlinear Dynamics; 2024;112(15)**:** 12907-12924.
21. Dominik Worf, Ali Khosronejad, Thomas Gold, Kevin Reiterer, Helmut Habersack, Christine Sindelar. Fluid structure interaction of a subaqueous pendulum: Analyzing the effect of wake correction via large eddy simulations. Physics of Fluids. 2022;34 (5).